Parametric Catastrophe Bonds for Tsunamis: CAT-in-a-Box Trigger and Intensity-Based Index Trigger Methods

Katsuichiro Goda,[a] Guillermo Franco,[b] Jie Song,[a] and Alin Radu[a]

This study presents a calibration of CAT-in-a-Box and intensity-based index trigger mechanisms for parametric tsunami catastrophe bonds. Trigger conditions for the former are based on fundamental event characteristics, such as earthquake location and magnitude, whereas those for the latter utilize tsunami wave height measurements at a series of observation stations. These solutions are illustrated for a building portfolio in Iwanuma City in Miyagi Prefecture, Japan, by considering a new seafloor observation network S-net off the Tohoku-Hokkaido coast of Japan. Performances of the two types of parametric solutions are quantitatively evaluated and compared with each other to discuss their advantages and disadvantages. [DOI: 10.1193/030918EQS052M]

INTRODUCTION

Reducing tsunami risks is a global challenge and is essential for achieving sustainable development of coastal areas around the world (Løvholt et al. 2014). Human, physical, and economic loss due to tsunamis can be devastating, as exemplified by destructive tsunamis during the 2004 Indian Ocean and the 2011 Tohoku, Japan, events. Physical protective measures, disaster education, and evacuation planning are all useful elements to improve the resilience of coastal communities. Regardless of the level of preparedness, however, monetary impacts are bound to ensue. Insurance is a conventional instrument to transfer financial risks arising from natural disasters that aims to complement other mitigation efforts (Mossin 1968, Schlesinger 2000). Over the last two decades, the insurance market has evolved in its sophistication, notably opening the door to "alternative capital" sourced from investment entities rather than from traditional insurance and reinsurance companies (Mitchell-Wallace et al. 2017). This hybrid space between insurance and finance is often referred to as the "convergence" market. In order for this capital to find its way into insurance operations, the market needs tradeable securities. Packaging catastrophe risks in the form of a security (e.g., catastrophe or "CAT" bonds) has enabled agents in the convergence market to become active providers of capital at risk. The amount of money deployed by investors to provide risk protection has been growing over the years, and it is still on the rise.

Earthquake CAT bonds are financial products that transfer earthquake risk to the capital market. A single-purpose reinsurer collects funds (principal) from investors and issues CAT bonds. In cases in which pre-agreed/specified trigger conditions are met, the single-purpose reinsurer releases the principal to the sponsor; otherwise, the principal together with return

[a] Department of Civil Engineering, University of Bristol, Queen's Building, University Walk, Bristol, United Kingdom; Email: kgoda2@uwo.ca (K. G.)
[b] Guy Carpenter, Marsh & McLennan Innovation Centre, Dublin, Ireland

higher than typical securities is paid back to the investors when the bonds mature. CAT bonds have advantages and disadvantages with respect to conventional risk transfer methods (Cummins 2008) and take many different aspects. In this work, we discuss a specific form of CAT bonds that are of a "parametric" nature, meaning that the outcome decision to pay after a destructive event is not through an insurance settlement process but on a series of physical parameters that can be measured. The settlement process can be costly as well as take a very long time because the insurance claims made by the insured need to be evaluated and verified by loss adjusters as well as engineers who are knowledgeable about earthquake damage. Investors without expertise in the loss settlement process prefer a parametric approach because it saves them the effort associated with adjusting losses and provides transparency. Sponsors, the beneficiaries of the bond payment, also like the transparency of parametric tools in addition to the potentially very high speed of payment. This aspect is particularly beneficial for mobilizing resources in emergency response and early-recovery phases of critical importance, as evidenced in the Christchurch scenario (King et al. 2014).

The main disadvantage of parametric CAT bonds is tied to the absence of a loss adjusting process. Since there is no assessment of the loss, there is an imperfect correlation between the actual losses experienced and the payments received. The difference between these two is usually referred to as basis risk. Basis risk arises because the parameters involved in determining the payment are insufficient to characterize the full consequences of the event. Since parametric risk transfer products are calibrated with numerical risk models, basis risk can also suffer from shortcomings in the models used. To refer to the limitations imposed by the parametric formulation, the terms of "trigger error" or "index error" are often used. On the other hand, "model risk" is used to refer to those imposed by the model.

Parametric approaches may be based on a few fundamental event characteristics (e.g., earthquake location and magnitude) or on a large number of intensity measurements, usually packaged into an index formulation. The former approach is referred to in the industry as a "CAT-in-a-Box" or "first-generation," whereas the latter approach is typically known as an "intensity-based index" or "second-generation" solution (Wald and Franco 2016). Both approaches are useful, and their optimal application setting depends on several factors, such as expertise of the parties using them, complexity of the portfolio at risk, and the availability and disposition of the instruments providing the required measurements. CAT-in-a-Box solutions make sense when simplicity and transparency are important and when the potential loss is difficult to assess (e.g., business interruption) or when the measurements required for second-generation index solutions are not available. In seismic regions where reliable observation/monitoring networks are in place to provide reliable intensity measurements over a large portion of the geography (e.g., California and Japan), intensity-based indices can be considered (Goda 2013, 2015, Pucciano et al. 2017). Local intensities near the sites of interest (e.g., peak ground accelerations or spectral accelerations calculated from recorded ground motion time histories) are, in general, good predictors of earthquake damage and loss and therefore typically increase the correlation between payment outcomes and actual loss. In other words, they have the potential to minimize basis risk and therefore constitute an appealing alternative.

Both parametric approaches require values of the trigger parameters to be reliably provided by a trusted third party shortly after an event, such as the U.S. Geological Survey and

the Japan Meteorological Agency. Intensity-based indices require these values to be provided for an extensive network of instruments, such as the K-NET and KiK-net systems in Japan. In the context of intensity-based indices for tsunamis, the deployment of a new seafloor observation network off the Tohoku-Hokkaido coast of Japan, S-net (http://www.bosai.go.jp/inline/; Kanazawa 2013), provides an exciting and unique opportunity to construct parametric solutions for risk transfer. The network, which will be operational in 2018, includes 150 ocean-bottom pressure sensors at both shallow- and deep-water areas, whose reported tsunami waves could be used to define tsunami loss intensity-based indices.

Although parametric earthquake solutions have been traded since 1997, no publicly advertised deal has yet addressed tsunami losses specifically, probably due to the scarcity of reliable catastrophe models for tsunami risk. Recently, Goda and De Risi (2017) have developed a new probabilistic tsunami loss estimation method by considering stochastic earthquake sources (Goda et al. 2014, 2016). The approach is based on a performance-based engineering framework (Cornell and Krawinkler 2000, Goulet et al. 2007), and allows carrying out probabilistic tsunami hazard-risk analysis at regional scale by accounting for various uncertainties, such as earthquake source, tsunami inundation, damage, and loss.

In this paper, we use the above-cited model to calibrate CAT-in-a-Box type and intensity-based index solutions to approximate tsunami losses. We use the fundamental event parameters (e.g., earthquake magnitude and location) for the first type of solution, as is customary (Franco 2010). We use the maximum tsunami wave height at a series of observation stations (mimicking the behavior of the imminently operational S-net) to calibrate a logistic regression model to define the parametric index mechanism. We construct these solutions considering several variations. For instance, CAT-in-a-Box triggers can be developed by considering different spatial sub-regions or a grid. Intensity-based indices can be defined using different numbers of stations to identify an optimal configuration of the network, similar to the analysis of Pucciano et al. (2017), for parametric earthquake loss approximations. We then compare the different solutions obtained and discuss advantages and disadvantages. As an illustration, a case study is presented for the coastal areas of Iwanuama City, Miyagi Prefecture, Japan, where major destruction occurred during the 2011 Tohoku tsunami (Fraser et al. 2013).

TSUNAMI LOSS DATA FOR DEVELOPING PARAMETRIC CAT BOND TRIGGER

This section presents the key features of a probabilistic tsunami loss model used to calibrate the parametric solutions introduced above. We first summarize the model's main components succinctly, noting that these are covered in detail by Goda and De Risi (2017). We then present a tsunami loss modeling case study for Iwanuma in Miyagi Prefecture of Japan. We use these loss results to make a series of preliminary observations regarding the correlation between loss and the main physical parameters of earthquake rupture as well as with the maximum tsunami wave heights at a network of measuring stations. These observations will assist us in assessing the potential utility of the two types of parametric solutions studied in this paper for the case study at hand.

PROBABILISTIC TSUNAMI LOSS MODEL FOR A BUILDING PORTFOLIO

The model used consists of eight modules or sub-models. Five of these components are used to determine the tsunami inundation hazard across the affected region. The three remaining modules consist of an exposure database, a vulnerability module, and a loss calculation engine (see Figure 1).

Seismicity Model

The expected distribution of earthquake occurrences is characterized in accordance with the seismic hazard model for the Tohoku region proposed by the Headquarters for Earthquake Research Promotion (2013). Using earthquake catalog data in the Tohoku region, the annual occurrence rate of tsunamigenic earthquakes having M_w7.5 is estimated to be 0.08 per year. A Gutenberg–Richter curve is fitted to obtain the recurrence values for events between M_w7.5 and M_w9.1. This magnitude range is discretized with an interval of 0.2.

Fault Model

A regional fault source model is developed by extending the fault plane geometry for the 2011 Tohoku earthquake considered by Satake et al. (2013) covering an area 650 km long by 250 km wide. The strike angle is assumed constant at 193°, while the dip angle is considered variable along the subducting plate interface, gradually steepening from 8° to 16° in the down-dip direction. The eastern boundary of the fault plane model approximately coincides with the Japan Trench. To characterize heterogeneous earthquake slip over the fault plane, the source zone is discretized into sub-faults of 10 km by 10 km in area.

Scaling Model

Eight source parameters are used to characterize the earthquake rupture in terms of fault geometry and slip distribution (Goda et al. 2016). The geometrical parameters, i.e., fault width W and fault length L, determine the size of the fault rupture, and the position of the synthesized fault plane is determined such that it fits within the source zone. The slip parameters, i.e., mean slip D_a and maximum slip D_m, specify the earthquake slip statistics over the fault plane. The Box-Cox power transformation parameter λ determines how the slip values are marginally distributed over the fault plane and is used to capture non-uniform characteristics of earthquake slip (Goda et al. 2014). The spatial slip distribution

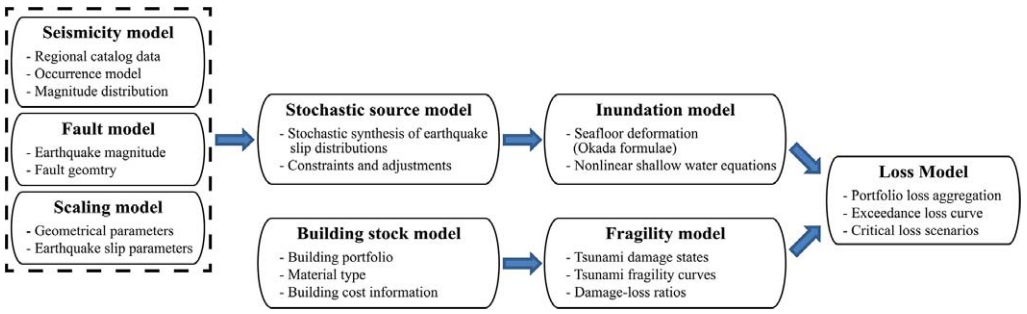

Figure 1. Probabilistic tsunami loss estimation procedure.

parameters, i.e., the correlation length along dip/strike, A_d and A_s, and Hurst number H, are used to characterize the heterogeneity of earthquake slip over the fault plane, represented by the von Kármán wavenumber spectrum, which specifies how slip values are spatially correlated over the fault plane.

Stochastic Source Model

After sampling the spatial slip distribution parameters, a random slip field is generated using the Fourier integral method (Pardo-Iguzquiza and Chica-Olmo 1993, Goda et al. 2014), where the amplitude spectrum is represented by the von Kármán spectrum and its phase is uniformly distributed between 0π and 2π. To achieve a slip distribution with realistic right-heavy tail features, the synthesized slip distribution is converted via Box-Cox power transformation using the simulated value of λ. The transformed slip distribution is then adjusted to achieve the target mean slip D_a and to avoid very large slip values exceeding the target maximum slip D_m.

Inundation Model

To evaluate the tsunami intensity measures (inundation depths) at building locations, we solve the nonlinear shallow water equations (Goto et al. 1997). The initial water surface elevation due to earthquake rupture is evaluated based on formulas by Okada (1985) and Tanioka and Satake (1996). The computational domains are nested at four grid resolutions: 1350 m, 450 m, 150 m, and 50 m domains (note that land elevation data are represented by 50-m grid points). The simulated tsunami wave heights at these grid points are used to estimate inundation depths at building locations. Tsunami inundation simulations are conducted for all stochastic sources.

Building Stock Model

The exposure model characterizes the assets at risk within a region of interest. The building dataset used in this study is based on the post-2011-Tohoku tsunami damage data compiled by the Ministry of Land Infrastructure and Transportation (MLIT). The data contain information on building locations, damage levels based on post-tsunami surveys (minor, moderate, major, complete, collapse, and washed away, as defined by the MLIT), structural material (reinforced concrete, steel, wood, and others), and the number of stories. We use regional statistics of unit building costs and floor areas to estimate the cost of the buildings, both of which are modeled as lognormal variables.

Fragility Model

Tsunami fragility functions relate tsunami hazard intensity measures (inundation depths) to probabilities of attaining different damage states. In this study, we adopt the empirical model by De Risi et al. (2017), which is based on the tsunami damage data gathered by the MLIT. Sampling a uniform random variable ranging between 0 and 1 and subsequently comparing this simulated value with the damage state probabilities, the corresponding tsunami damage state can be determined (i.e., minor, moderate, extensive, complete, or collapse). According to the MLIT, damage ratios for the minor, moderate, extensive, complete, and collapse damage states are assigned as: 0.03–0.1, 0.1–0.3, 0.3–0.5, 0.5–1.0, and 1.0, respectively.

Loss Model

The monetary loss associated with the tsunami effect on a building is calculated simply by sampling the total replacement cost from the lognormal distribution and multiplying it by the damage ratio determined from the fragility analysis. We repeat the procedure for all buildings in the portfolio in order to obtain the total tsunami loss for each event in the stochastic sample. These loss samples can then be used to construct the conditional probability distribution functions of the total portfolio loss for a given magnitude range, and to develop the unconditional probability distribution function of tsunami loss by considering regional seismicity.

CASE STUDY FOR IWANUMA

We use this tsunami loss model to generate datasets of loss events with their corresponding tsunami hazard characteristics for Iwanuma in Miyagi Prefecture, Japan (Figure 2a). The particular building portfolio includes 6,791 buildings located in low-lying coastal plain areas of Iwanuma City (Figure 2b), consisting of 137 reinforced concrete, 558 steel, and 6,096 wooden structures. This is the same building portfolio considered by Goda and De Risi (2017). The hazard component considers a total of 4,000 stochastic source models corresponding to 500 stochastic simulations for each of eight earthquake magnitude ranges between M_w7.5 and M_w9.1 with 0.2 interval.

We extract various characteristics from the stochastic event set, such as magnitude and representative source locations, which are useful for developing the CAT-in-a-Box triggers.

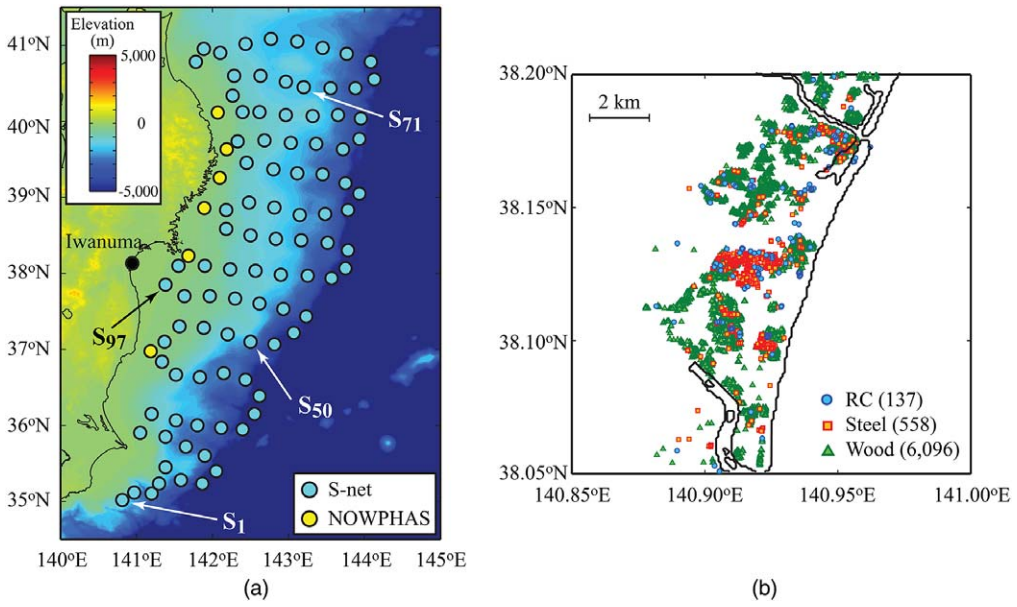

Figure 2. (a) Locations of Iwanuma and tsunami observation stations off the Tohoku coast (NOWPHAS and S-net) and (b) building inventory in Iwanuma.

In this study, four different definitions of the representative source location are investigated; the geometrical centroid and three variations of the slip centroid (i.e., the slip threshold is determined as mean slip multiplied by a factor of 0, 1.0, and 3.0). This setup is to investigate the effects of different definitions of representative source locations on the CAT-in-a-Box triggers due to non-uniqueness of representative source locations for mega-thrust subduction earthquakes (Goda and Atkinson 2014).

To obtain an array of simulated wave height observations, we consider a total of 99 stations, including six GPS buoy stations currently in operation off the Tohoku region as part of the NOWPHAS system (Kawai et al. 2013) and 93 S-net stations that will be operational imminently (Kanazawa 2013). Figure 2a shows the locations of the S-net instruments in the vicinity of the region analyzed. The tsunami simulations yield wave height profiles at the 99 stations for the 4,000 stochastic source models considered.

PRELIMINARY INVESTIGATIONS OF TSUNAMI LOSS DATA

CAT-in-a-Box triggers prominently use the magnitude and location of the event, since these are obtainable values from local and international agencies quickly after an event. This assumes that the correlation between these parameters and the loss is at least sufficiently strong. To illustrate this, Figure 3a shows a scatter plot of tsunami loss in Iwanuma against earthquake magnitude. We can clearly see that the tsunami loss drastically increases with earthquake magnitude, as one would expect, but for a given magnitude range, the scatter in the data is rather large. This is expected since the magnitude in isolation (without accounting for the location of the event) is a rather poor predictor of loss.

To display the potential of location-related parameters to correlate with loss, Figure 3b shows the spatial distribution of the slip centroids (zero-slip threshold) for the 4,000 source models. As mentioned above, for mega-thrust earthquakes, it is not trivial to define single representative location because of the large extent of earthquake rupture. Regardless of results for other definitions of earthquake source location (e.g., geometrical centroid and slip centroids based on different slip thresholds), observations that can be obtained from other representative locations are similar (note: variability of the source location tends to be smaller for the geometrical centroid, whereas it tends to be greater when the slip centroid with a larger slip threshold is considered). The data indicate, predictably, that seismic events causing large tsunami loss tend to be near the center of the rupture plane or in the shallower part of the subduction interface.

To further investigate this point, consider the distance and azimuth between Iwanuma and the slip centroids for all 4,000 source models. The results are shown in Figure 3c and Figure 3d, respectively. Because the strike of the fault rupture plane is constant at 193°, an azimuth range between 100° and 105° approximately corresponds to the direction perpendicular to the considered rupture boundary on the Japan Trench side. The results are useful for understanding the effects of the source-to-site distance and the orientation of the source with respect to the site. Although some general trends can be observed (e.g., when the distances are less than 200 km and when the azimuth angles are near 100°, the tsunami loss tends to be greater), both figures show large variability (i.e., low correlation) with tsunami loss.

Intensity-based indices can be designed to make use of the maximum tsunami wave heights at the observation stations. Figure 4 shows the scatter plots of tsunami loss in Iwanuma against the maximum tsunami wave heights at four stations: S_{97}, S_{50}, S_1, and S_{71}

(see Figure 2a for locations of the four stations). S_{97} is the closest station from Iwanuma, and the tsunami wave height at S_{97} is expected to be better correlated with the tsunami loss there. S_{50} is in deep-water areas at an azimuth angle of about 100°, and it is located in the large slip areas near the Japan Trench, thus a moderate correlation is anticipated. S_1 and S_{71} are far from Iwanuma, and the correlation is expected to be low. The results shown in Figure 4 corroborate this intuition. The tsunami wave at the closest site (S_{97}) is reasonably well correlated with the tsunami loss, followed by S_{50}. On the other hand, the maximum tsunami wave heights at S_1 and S_{71} are not informative to predict the tsunami loss in Iwanuma.

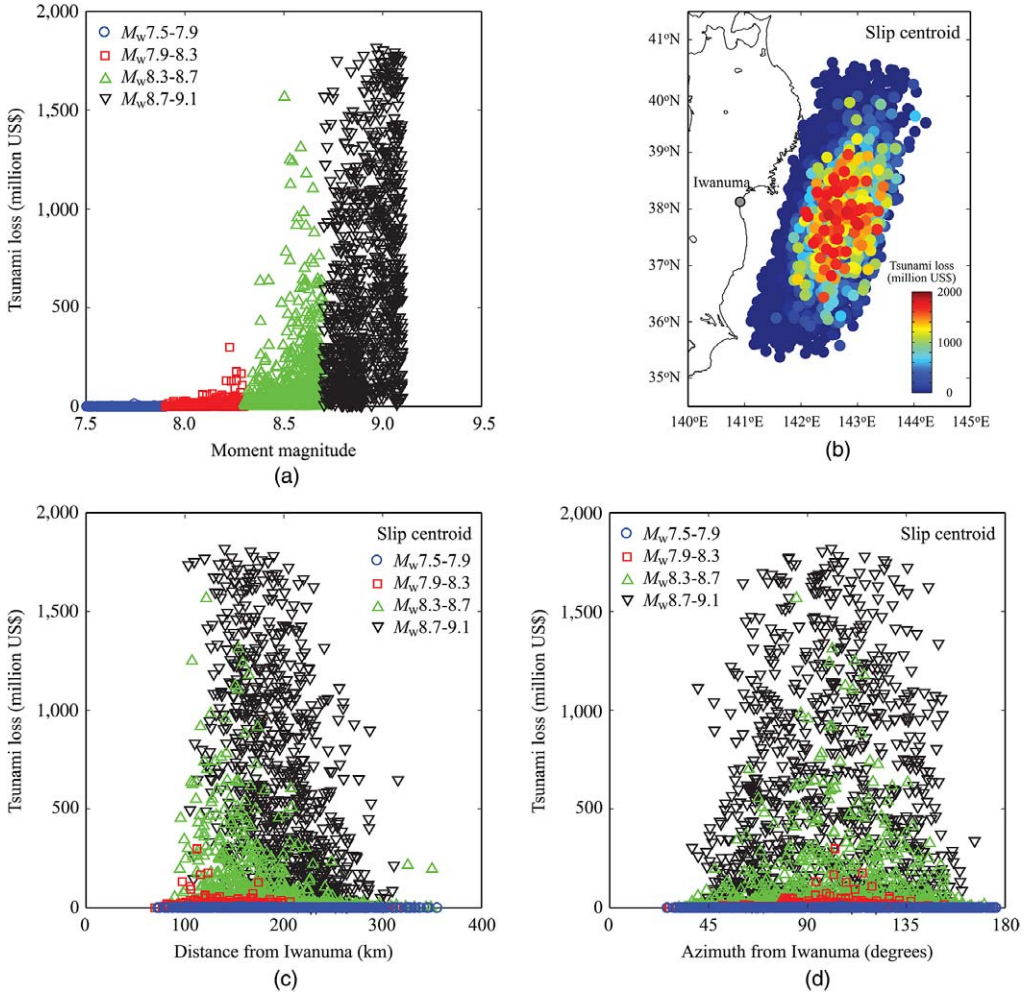

Figure 3. (a) Scatter plot of tsunami loss in Iwanuma and earthquake magnitude; (b) distributions of the slip centroid of earthquakes; (c) scatter plot of tsunami loss in Iwanuma and distance from Iwanuma to the slip centroid; and (d) scatter plot of tsunami loss in Iwanuma and azimuth between Iwanuma and slip centroid. The slip centroid is obtained by considering zero-slip threshold.

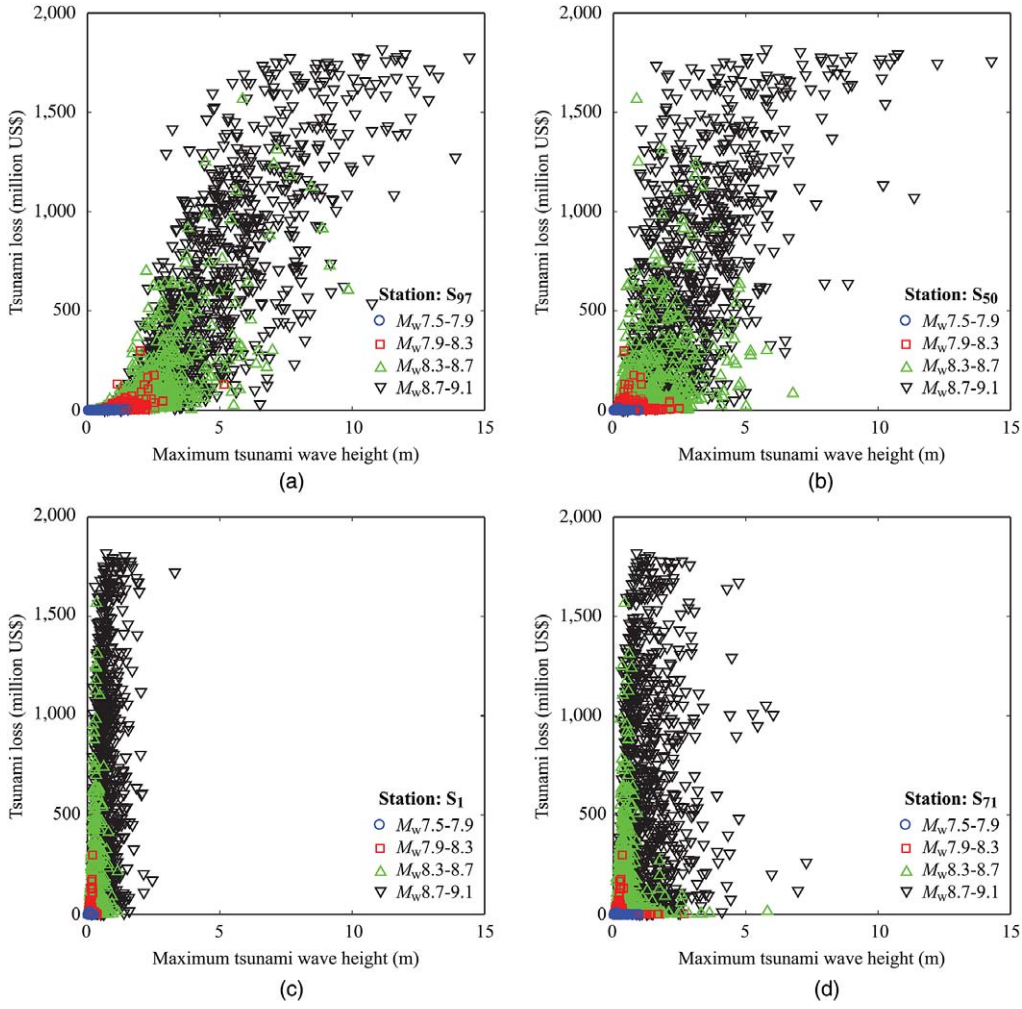

Figure 4. Scatter plots of tsunami loss in Iwanuma and maximum tsunami wave height: (a) S_{97}; (b) S_{50}; (c) S_1; and (d) S_{71}. See Figure 2a for locations of the four stations.

These preliminary observations indicate that carefully selected intensity parameters may correlate with loss better than the key fundamental event parameters of magnitude and location in isolation (Pucciano et al. 2017). We will investigate in more detail these assertions as we design actual parametric prototypes using both approaches.

TRIGGER CALIBRATION METHOD

As pointed out above, parametric triggers need to achieve a high level of correlation with loss (i.e., reducing basis risk). The process through which we minimize basis risk can also be interpreted as the "calibration" of the triggers. In calibrating parametric trigger methods, it is important that the developed trigger mechanisms are robust with regard

to unforeseen situations. Thus, as part of trigger calibration, the ability of the developed trigger method needs to be tested against unseen data. For this purpose, a repeated cross-validation scheme is incorporated in the trigger calibration process (e.g., Kim 2009). More specifically, a repeated ten-fold cross-validation is implemented, where the entire dataset (i.e., 4,000 pairs of portfolio loss data and earthquake/tsunami hazard information) is divided into two parts: fitting data and testing data. For the ten-fold cross-validation, the split between the fitting and testing data is 3,600 and 400. This split is repeated ten times by considering all combinations of the "9 versus 1" split. The final performance of the trigger method is evaluated based on the average performance using the testing dataset.

CAT-IN-A-BOX TRIGGER METHOD

There are four basic steps to calibrate the CAT-in-a-Box trigger mechanisms:

1. The first step is to define an earthquake hazard region for which bond triggers are designed. This depends on a sponsor's motivation/interest in setting up CAT bonds to protect from future catastrophic losses. For our case study in Iwanuma, a near-shore tsunamigenic source region off the Tohoku coast can be selected (e.g., Figure 2a).
2. The source region of major seismic events is discretized into sub-regions with different sizes. A careful selection of the size of sub-region is important because the earthquake rupture area increases rapidly with earthquake magnitude, and the trigger mechanisms become complex with the decrease of the sub-region size. In addition, the representative source is defined by adopting one of the four different definitions of the representative source location (e.g., geometrical centroid and slip-based centroid).
3. Trigger conditions for individual sub-regions in terms of earthquake magnitude are determined by minimizing the total trigger errors using the fitting data. The magnitude range is defined for discrete threshold values from M_w7.5 to M_w9.0 with 0.1 interval. The focal depth is not used as the location parameter because it is implicitly accounted for by the location of sub-regions, which are defined on the subducting plate interface. Since the focal depth is not considered as the trigger parameter, an exhaustive search of optimal magnitude threshold for individual sub-regions can be implemented without significant computational efforts. The trigger errors based on testing data are evaluated using the identified magnitude threshold. This is iterated for all sub-regions.
4. To implement ten-fold cross-validation, the above evaluation is carried out ten times for different combinations of fitting and testing data.

Furthermore, to investigate the effects of the parameter setting, variations of the parameter settings (e.g., grid size of sub-regions and definition of representative source location) are considered to compare the trigger performances of different CAT-in-a-Box trigger methods.

The procedure mentioned in the preceding paragraph is demonstrated for the building portfolio in Iwanuma by considering a loss threshold for the bond trigger of U.S. $100 million

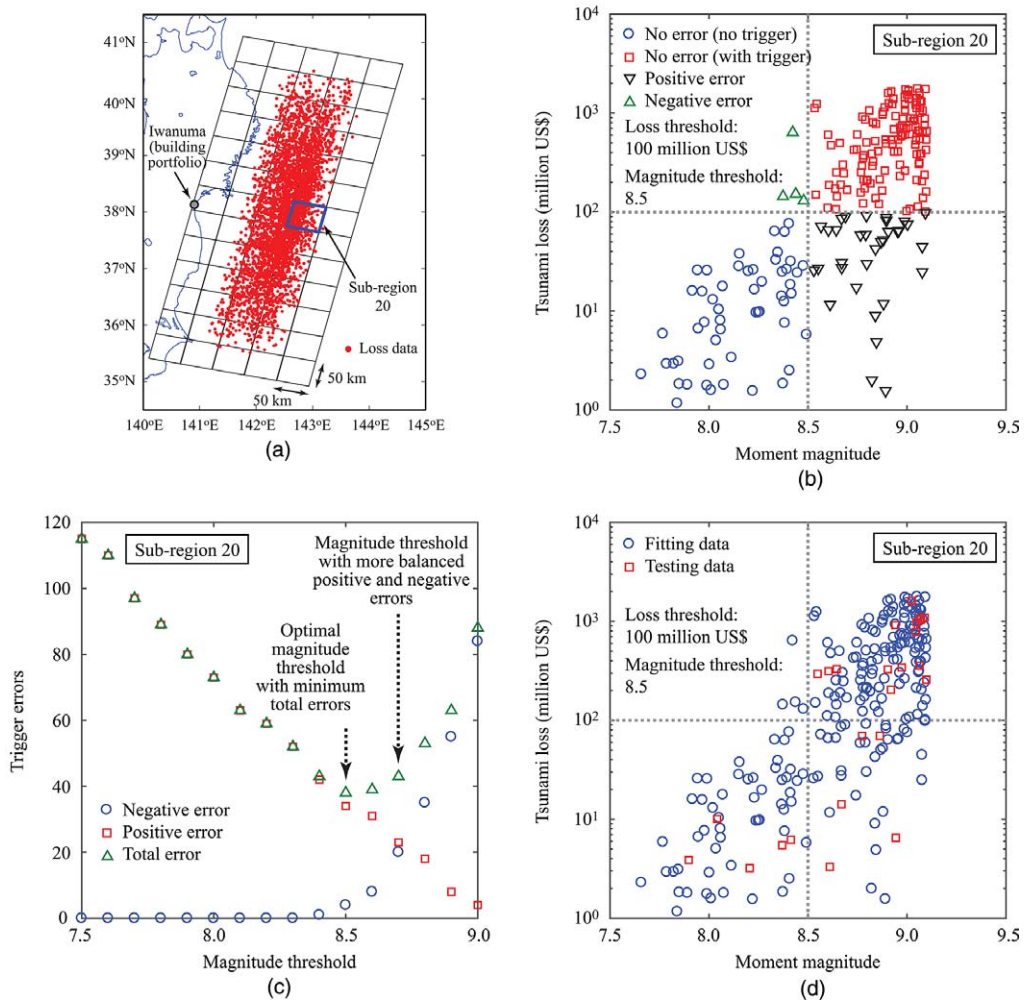

Figure 5. (a) Target source region and discretized sub-regions (50 by 50 km) for the CAT-in-a-Box triggers; (b) portfolio loss in Iwanuma versus moment magnitude for sub-region 20 based on the fitting data; (c) trigger errors versus magnitude threshold for sub-region 20 based on the fitting data; and (d) portfolio loss in Iwanuma versus moment magnitude for sub-region 20 based on the fitting and testing data.

(see Figure 5). Consider a sub-region 20 that is indicated by a blue polygon in Figure 5a. In total, 242 loss data, out of 3,600 fitting data, fall within this sub-region. The scatter plot of the tsunami loss data and the corresponding moment magnitude is shown in Figure 5b. By considering M_w8.5 as a trial magnitude threshold for this sub-region, the fitting data can be classified into four cases: no error without trigger (blue circle), no error with trigger (red square), positive error (black inverted triangle), and negative error (green triangle). Hence, for this case, the total, positive, and negative errors are 38, 34, and 4, respectively.

By changing the trial magnitude threshold value from M_w7.5 to M_w9.0, curves displaying total/positive/negative trigger errors versus magnitude threshold can be obtained for sub-region 20 (Figure 5c). From this result, an optimal magnitude threshold for sub-region 20 that minimizes the total trigger errors is identified as M_w8.5.

We need to develop the CAT-in-a-Box trigger mechanisms so they are "robust," i.e., they perform well for sets of data beyond the data used for calibration. Performance is defined as minimizing basis risk and providing a reasonable balance between false positive and false negative trigger outcomes. Figure 5d illustrates the performance of the previous trigger design for the testing data with total, positive, and negative errors of 5, 5, and 0, respectively. Figure 5c illustrates how the selection of a magnitude threshold of M_w8.7 can achieve a balanced distribution of positive and negative trigger errors with slightly greater total errors. Note that the robust performance of the trigger is tied to the size of the grid used to define the sub-regions. When the grid size is set to relatively small values, overfitting of the magnitude threshold can occur, resulting in poor trigger performance against a new sample of testing data.

INTENSITY-BASED INDEX TRIGGER METHOD

The key feature of the intensity-based index triggers is the use of observable tsunami hazard parameters, such as maximum tsunami wave heights at GPS buoys and ocean-bottom pressure sensors (Figure 2a), instead of earthquake source parameters (e.g., magnitude and location). Goda (2013) pointed out that the intensity-based index method is likely to perform better than the CAT-in-a-Box method because intensity parameters are more correlated with losses.

The intensity-based index method is based on logistic regression analysis (Agresti 2007):

$$f(x) = \frac{1}{1 + \exp(-(\beta_0 + \beta_1 x_1 + \cdots + \beta_k x_k))} \tag{1}$$

where $x_1,\ldots,x_k$ are the explanatory variables, and $\beta_0,\ldots,\beta_k$ are the regression coefficients. In the context of parametric CAT bonds, the explanatory variables are the maximum tsunami wave heights at observation stations. Prior to the logistic regression, the portfolio tsunami loss needs to be converted to binary variables using the trigger loss threshold. It is important to note that the fitted logistic regression model produces a value between 0 and 1 (i.e., non-binary). Therefore, a reasonable method to transform from non-binary output to binary output is needed. A simple approach is to round the number to 0 or 1 by considering a threshold of 0.5. Alternatively, the rounding threshold can be changed to minimize the differences between positive and negative trigger errors (Goda 2013).

To demonstrate the above intensity-based index method, logistic regression results based on the maximum tsunami wave height at S_{97} are shown in Figure 6a (see Figure 2a for the location of S_{97} and Figure 4a for the scatter plot of the tsunami loss and the maximum tsunami wave height). The considered trigger loss threshold is U.S. $100 million (same as Figure 5). In the figure, input data are 3,600 data pairs of binary loss trigger indicators and corresponding maximum tsunami wave heights (indicated by blue dots, noting that they are plotted on horizontal lines at 0.0 and 1.0 and overlap one another). The red squares

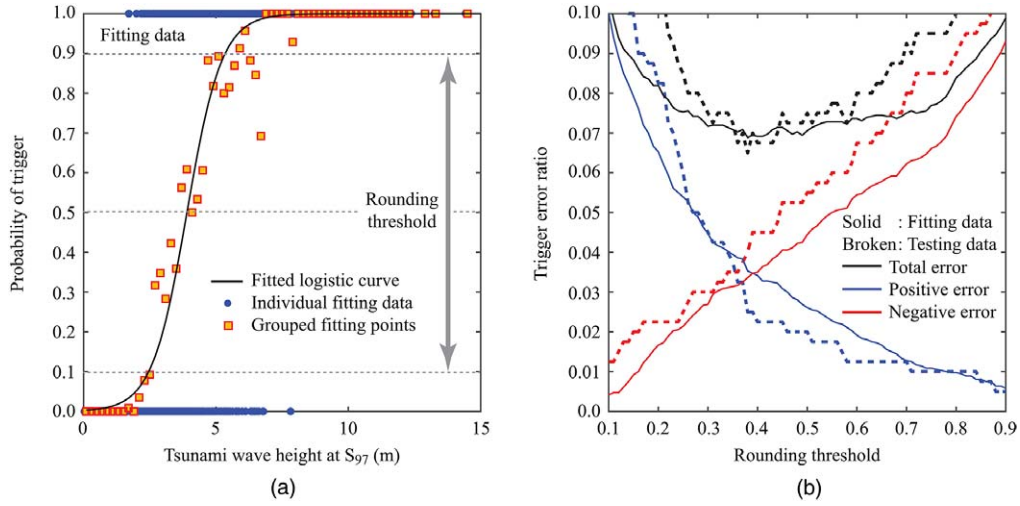

Figure 6. (a) Logistic regression model calibrated using the maximum tsunami wave height at S_{97} (see Figure 2a) and (b) optimization of the rounding threshold by considering both total trigger errors and differences of positive and negative trigger errors.

are the proportions of loss-triggering data points for given bins of the maximum tsunami wave height. The logistic model fits well with the grouped data points. The trigger performance of the logistic model is evaluated using the unseen testing data. Once the logistic model is determined, the threshold for rounding to transform continuous output to binary output can be optimized by taking into account both total trigger errors and differences of positive and negative trigger errors. This analysis step is demonstrated in Figure 6b. For this example, the rounding threshold of about 0.4 can achieve relatively small total trigger errors with similar positive and negative trigger errors. The results shown in Figure 6 are for a specific cross-validation case; for the repeated ten-fold cross-validation, the preceding analysis is repeated ten times, and the overall performance of the intensity-based index method can be evaluated as the average results from ten sets of testing data.

The simplest form of the intensity-based index trigger mechanism is to use the maximum tsunami wave height at a single station, whereas the model can be extended to consider tsunami hazard parameters at multiple stations. Employing the tsunami hazard information at multiple locations is likely to improve the trigger performance; however, the degree of the improved performance may not be significant when enough observation stations are included in the logistic regression model. This leads to an investigation of optimal configuration of an observation network for a parametric CAT bond trigger; see Pucciano et al. (2017) on the loss predictive power of a given network of stations.

To develop the multiple-station trigger methods, two approaches are considered in this study. The most rigorous approach is to evaluate all combinations of observation stations exhaustively. For the observation system consisting of 99 stations (i.e., NOWPHAS and S-net; see Figure 2a), there are 99, 4,851, and 156,849 combinations of stations when the number of stations to be used for defining the trigger mechanisms is set to 1, 2, and 3, respectively.

The number of combinations increases significantly with the increase of the number of stations in the trigger network. To avoid an excessive number of trigger performance evaluations, an approximate method is to identify the least trigger error station sequentially (referred to as the sequential optimization method hereafter). For the case of the number of stations in the network equal to 3, a station that results in the best trigger performance can be identified by comparing the results for all 99 stations. Subsequently, the second-best station can be identified by evaluating 98 combinations of the paired stations (note: one station is fixed at the best station from the previous stage). The procedure can be repeated to identify the third-best station by evaluating 97 combinations of the triple stations (note: two stations are fixed at the best and the second-best stations from the preceding stages). The sequential optimization method reduces the number of performance evaluations drastically.

RESULTS

The main results of developing the CAT-in-a-Box and intensity-based index trigger methods are presented in this section by considering the case study in Iwanuma. Three tsunami loss levels are focused upon: U.S. $50 million, $300 million, and $700 million, which approximately correspond to 200-year, 500-year, and 1,000-year return periods in terms of aggregate tsunami loss for the building portfolio in Iwanuma. The results are based on repeated ten-fold cross-validation. As the main trigger performance metric, the average trigger error ratio, which is calculated as the total trigger errors divided by the total number of data points used for the assessment, is adopted. Because this is a normalized quantity, the results for fitting and testing data can be compared directly.

CAT-IN-A-BOX TRIGGER METHOD

The magnitude trigger thresholds are evaluated by considering different sub-region sizes from 10 km to 150 km. To illustrate the spatial distribution of the calibrated magnitude trigger thresholds, results for three sub-region sizes, i.e., 20 km by 20 km, 50 km by 50 km, and 100 km by 100 km, are shown in Figure 7a, Figure 7b, and Figure 7c, respectively. For each panel, three loss levels in terms of 200-year, 500-year, and 1,000-year return periods are considered to examine whether the trigger performance depends on the loss level. The magnitude threshold levels tend to increase with the return period, which is expected from the preliminary investigations. With the increase of the sub-region size, local variability of the magnitude threshold values decreases, in addition to their spatial resolution. These features may be beneficial from viewpoints of both sponsors and investors in understanding trigger conditions in a simple way.

To provide a more complete overview of the results for different sub-region sizes, average trigger error ratios for the three return period levels by considering the slip centroid with zero-slip threshold as representative source location are evaluated, and the results are summarized in the online Appendix (Table A1). In the table, for a given calibration setting, results for both fitting and testing data are included to inspect the problems related to over-calibration of trigger magnitude thresholds. The detailed results indicate that when the sub-region size is 10 km, the average trigger errors for the fitting data are the smallest (5% to 6%), while the corresponding average trigger errors for the testing data are the largest (18% to 19%). With the increase of the sub-region size (e.g, from 10 km to 150 km), the average trigger errors for the fitting data gradually increase (as expected), whereas the average trigger errors for

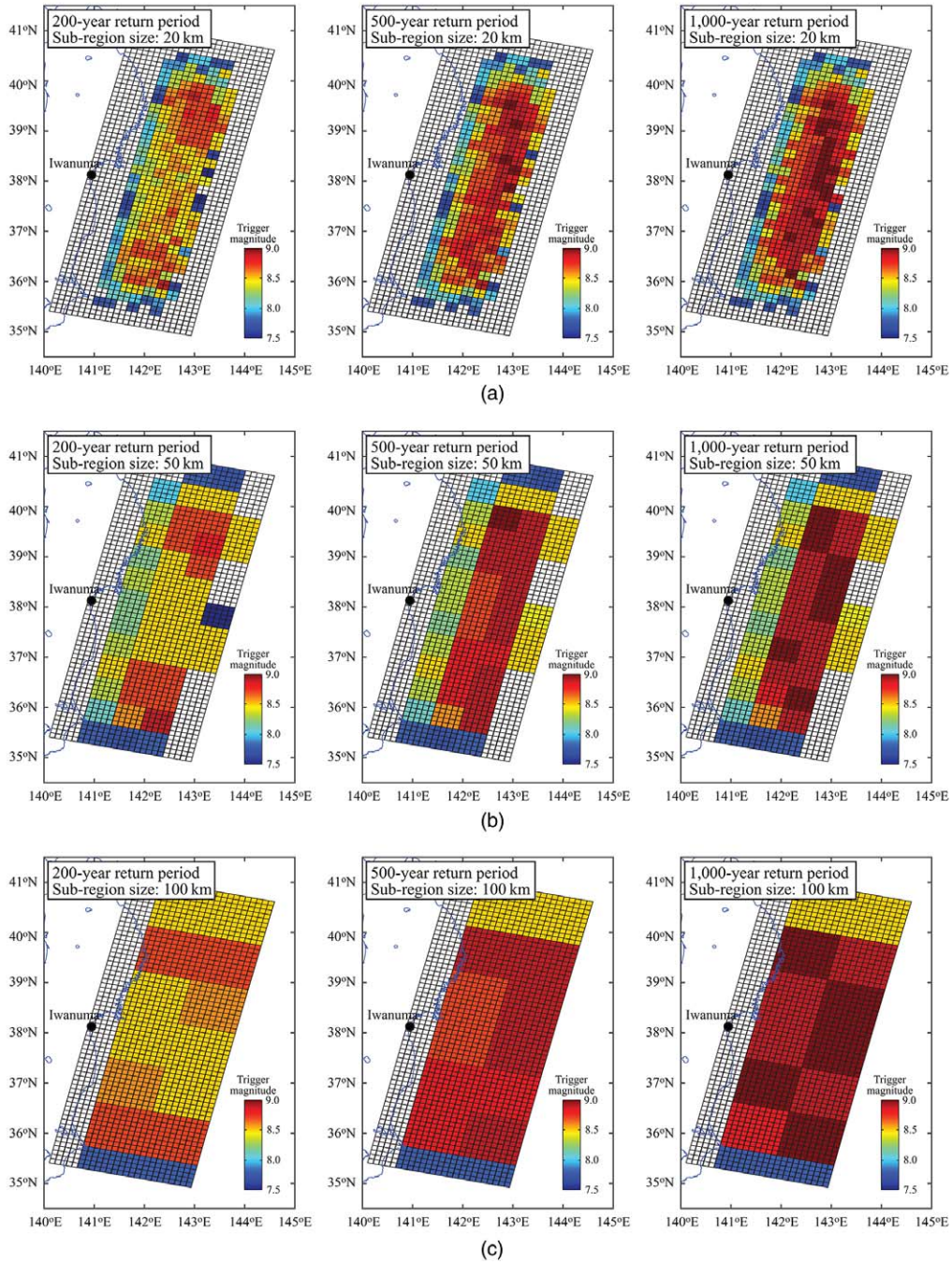

Figure 7. Magnitude thresholds for the 200-year, 500-year, and 1,000-year return periods by considering: (a) 20 km by 20 km sub-region size; (b) 50 km by 50 km sub-region size; and (c) 100 km by 100 km sub-region size. The base grid size is 10 km by 10 km.

the testing data decrease. A balanced situation for the average trigger errors for the fitting and testing data may be selected as a sub-region size of about 50 km, with the corresponding average trigger errors of 8% to 10%. Selecting too small sub-region sizes may lead to overfitting the tsunami loss results, and magnitude thresholds derived from such a small sub-region size may not produce robust results against unseen data. It is noteworthy that for a very large earthquake (M_w8 to M_w9 class), it is not trivial to define a source location at spatial resolutions of 10 km to 20 km, resulting in sharp changes of the magnitude threshold values, because the errors associated with the estimation of the representative earthquake locations may be greater than these spatial resolutions.

Moreover, to investigate the influence of adopting different definitions of representative source locations, average trigger error ratios for the 500-year return period level by considering the geometrical centroid and the slip centroids with threshold values of zero-slip, mean-slip, and 3×mean-slip are presented in online Appendix Table A2. The general trends of the average trigger error ratios in terms of sub-region size are similar for the four cases, resulting in about 8% to 10% errors when the sub-region size is 50 km or more. The trigger performance is slightly improved when the slip centroid with a large slip threshold is used. This may be because tsunami loss is more influenced by large-slip (asperity) distribution, than the overall fault geometry or the small slip distribution. The results confirm that the sub-region size is of critical importance in developing effective and robust CAT-in-a-Box trigger mechanisms.

INTENSITY-BASED INDEX TRIGGER METHOD

Results of the trigger performance of the intensity-based index method are discussed for two configurations of a tsunami wave observation system: single-station case and multiple-station case.

Single-Station Case

The single-station case is useful for demonstrating key features of the intensity-based index method by focusing on the trigger performance in terms of fitting versus testing data. For illustration, consider the results at S_{97} (closest to Iwanuma; see Figure 2a). Figure 8 shows trigger error ratios versus rounding threshold using the fitting and testing datasets at S_{97} for the 200-year, 500-year, and 1,000-year return period levels. The results are similar to those shown in Figure 6b. In each figure, ten sets of total/positive/negative trigger error ratio curves based on the ten-fold cross-validation are included. The results shown in Figure 8 indicate that for all three return period levels, individual trigger error ratio curves are consistent for the fitting data (i.e., calibration is done consistently for given fitting data), whereas the variability of the curves for the testing data is large. Overall, average trigger error ratio curves from the ten-fold cross-validation for the fitting and testing data are similar. The intensity-based index method achieves the least average trigger errors (about 5% to 7% depending on the return period level) when the rounding threshold is in the range between 0.3 and 0.5.

The trigger performance evaluation of the intensity-based index method for the single-station case is carried out for all 99 stations in the tsunami wave observation network (Figure 2a). Figure 9 shows the spatial distribution of the average trigger error ratios for the 200-year, 500-year, and 1,000-year return periods using the testing data. The markers with blue colors (smaller average trigger error ratios) are concentrated near Iwanuma and

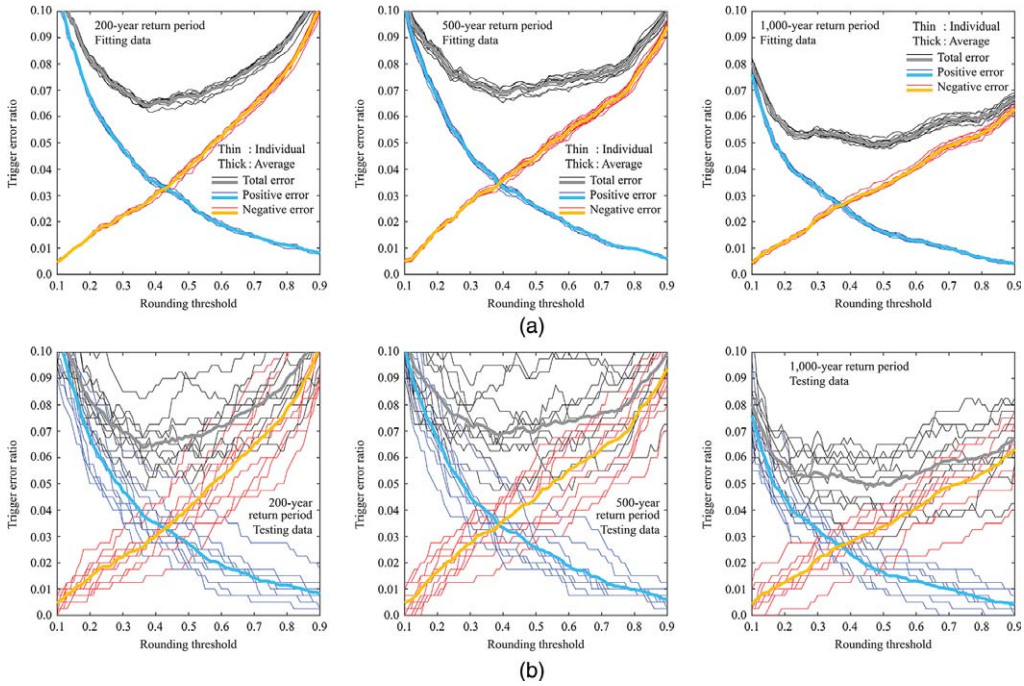

Figure 8. Trigger error ratios versus rounding threshold at S_{97} for the 200-year, 500-year, and 1,000-year return periods by using: (a) fitting data; and (b) testing data.

in offshore areas directly facing Iwanuma, whereas those with yellow-to-red colors (larger average trigger error ratios) are at stations relatively far from Iwanuma (both south and north of Iwanuma). The results corroborate the preliminary results and conjectures discussed for Figure 4. Importantly, the average trigger errors near Iwanuma are smaller than those attained by the CAT-in-a-Box method. We emphasize that shifting the rounding threshold can achieve a balanced distribution of positive and negative trigger errors, which is attractive for both sponsors and investors.

The results shown in Figure 9, in comparison with the results presented in the previous section on the CAT-in-a-Box trigger method, indicate that when the observation station near or in regions directly facing the target building locations is not available, the average trigger error ratio can be large, exceeding that of the CAT-in-a-Box trigger method (8%–10%, i.e., green to red colors in Figure 9). In such situations, the CAT-in-a-Box method may be a more robust procedure to determine the CAT bond trigger. In other words, the spatial distribution of buildings and compositions of buildings in terms of material and height are important aspects in calibrating an effective bond trigger mechanism.

Multiple-Station Case

Incorporating more tsunami hazard information in the parametric trigger mechanisms will result in improved trigger performance in comparison with the single-station case.

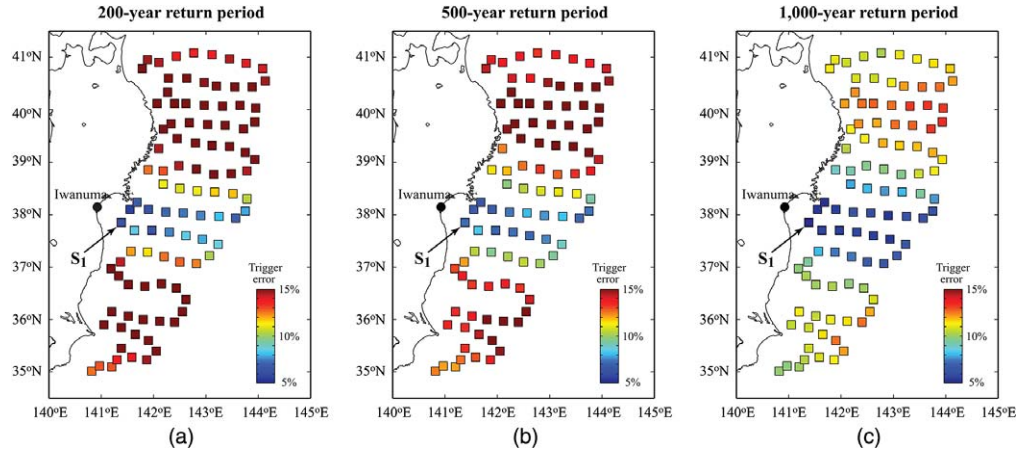

Figure 9. Spatial distribution of the average trigger error ratios for the single-station case: (a) 200-year; (b) 500-year; and (c) 1,000-year return periods.

It is also likely that the increment of the improved performance becomes smaller when a sufficient number of stations are already included in the trigger mechanisms. To investigate such aspects of the multiple-station parametric trigger method, the sequential optimization approach is adopted, noting that the exhaustive combination method of evaluating the trigger errors becomes practically infeasible when the number of stations consisting of the network becomes large.

Figure 10 shows the trigger error ratios (total, positive, and negative) versus the number of stations for the sequential optimization approach using the fitting and testing data. When the fitting data are considered (Figure 10a), the average trigger error ratios drop sharply in the first two to three stations and gradually decrease thereafter with the increase of the number of stations of the observation system. This is expected because use of more data should improve the fitting performance at least marginally. On the other hand, for the testing data (Figure 10b), the average trigger error ratios tend to drop significantly up to the inclusion of the first two to three stations in the model development; after this stage, the average trigger error ratios gradually increase with the increase of the number of stations in the network. Most importantly, the trigger performances of the multiple-station trigger method are superior to those of the CAT-in-a-Box method (3% to 4% versus 8% to 10%), highlighting the benefit of utilizing available tsunami hazard information for the parametric bond trigger instead of conventional earthquake source information.

The results discussed above are useful when the intensity-based index method is applied to other seismic regions where the observation systems in place are not as extensive as the Japanese S-net (note: the higher density of stations is to improve the capability for more accurate tsunami early-warning systems). More specifically, practical implications of the results for the case study in Iwanuma are that to achieve the accurate bond trigger based on intensity information, a few stations, which need to be carefully selected, may be sufficient—this may be affordable for many countries.

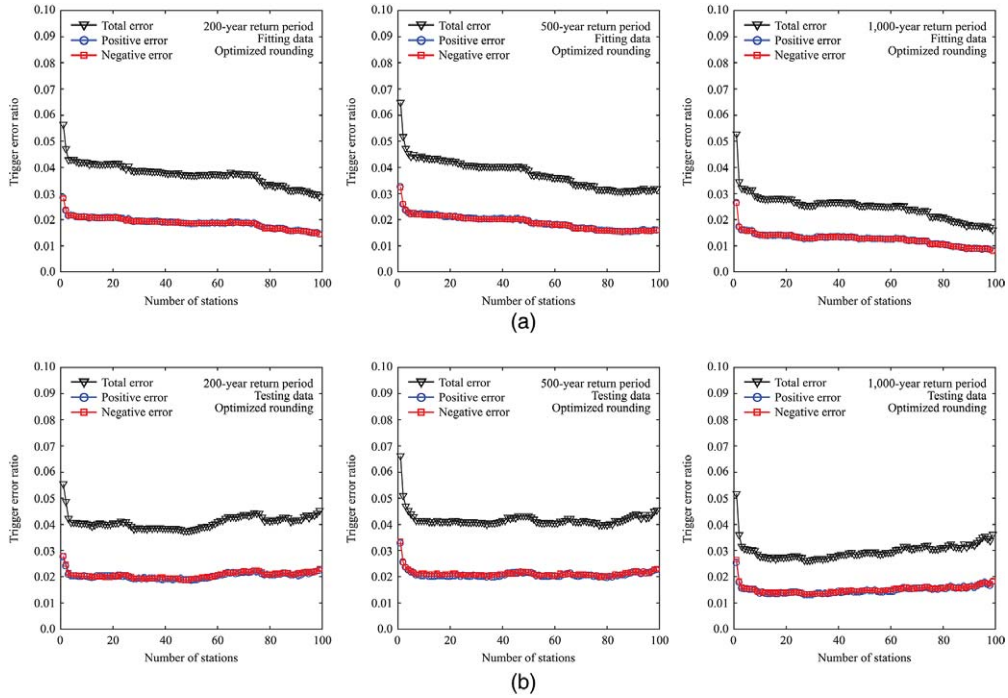

Figure 10. Average trigger error ratios (total, positive, and negative) versus the number of stations in the trigger network based on the sequential optimization approach using: (a) fitting data; and (b) testing data.

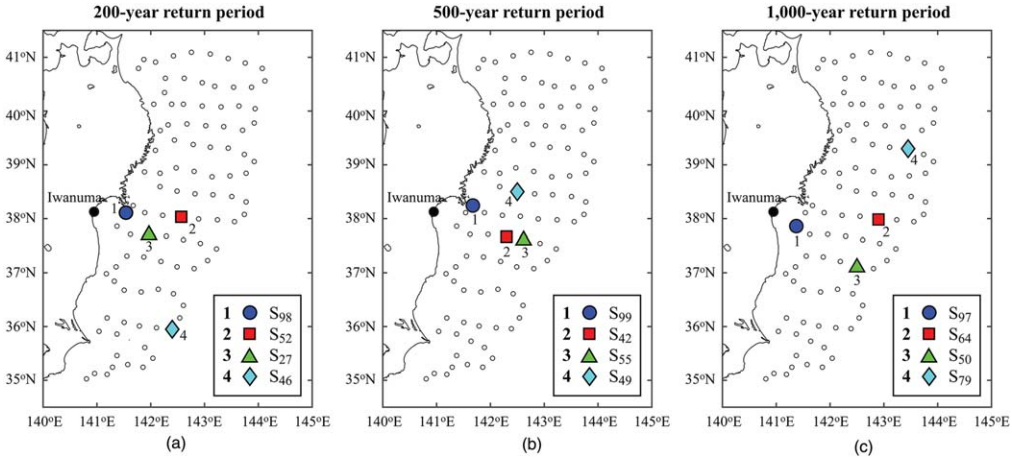

Figure 11. Locations of the best four stations based on the sequential optimization approach: (a) 200-year; (b) 500-year; and (c) 1,000-year return periods. The numbers indicated in the figure are the sequence order of the identified stations consisting of the optimized observation network.

Table 1. Comparison of the average triggering error ratios for the 200-year, 500-year, and 1,000-year return periods using the exhaustive combination approach and the sequential optimization approach

		200-year return period				500-year return period				1,000-year return period			
Exhaustive combination	Ave. trigger error ratio	**0.056**	0.063	0.065	0.067	**0.066**	0.068	0.068	0.071	**0.052**	0.052	0.053	0.054
1 Station	Station ID 1	**98**	24	97	27	**99**	24	98	27	**97**	99	66	98
Exhaustive combination	Ave. trigger error ratio	0.045	0.047	**0.049**	0.050	**0.051**	0.051	0.053	0.053	**0.036**	0.037	0.038	0.038
2 Stations	Station ID 1	52	40	**52**	27	**42**	64	42	62	**64**	27	73	62
	Station ID 2	97	97	**98**	52	**99**	97	88	99	**97**	64	97	64
Exhaustive combination	Ave. trigger error ratio	0.041	**0.042**	0.043	0.043	**0.047**	0.047	0.048	0.049	**0.032**	0.032	0.033	0.033
3 Stations	Station ID 1	40	**27**	52	35	**42**	42	42	23	**50**	50	62	64
	Station ID 2	52	**52**	97	52	**55**	64	97	42	**64**	73	64	73
	Station ID 3	97	**98**	99	97	**99**	99	99	99	**97**	97	99	97
Exhaustive combination	Ave. trigger error ratio	**0.041**	0.041	0.041	0.041	**0.045**	0.046	0.046	0.046	0.030	0.031	0.031	**0.031**
4 Stations	Station ID 1	**27**	40	14	19	**42**	42	42	42	60	8	49	**50**
	Station ID 2	**46**	52	27	27	**49**	46	54	52	62	62	62	**64**
	Station ID 3	**52**	76	52	52	**55**	64	64	97	64	64	64	**79**
	Station ID 4	**98**	97	98	98	**99**	99	99	99	99	99	99	**97**
Sequential optimization	Ave. trigger error ratio	**0.056**	**0.049**	**0.042**	**0.041**	**0.066**	**0.051**	**0.047**	**0.045**	**0.052**	**0.036**	**0.032**	**0.031**
	Station ID 1–4	**98**	**52**	**27**	**46**	**99**	**42**	**55**	**49**	**97**	**64**	**50**	**79**

To inspect the spatial distribution of the selected stations for the multiple-station trigger method, Figure 11 shows the locations of the top four stations identified based on the sequential optimization method. The figures indicate that the second-best and/or third-best stations are close (but not side by side) to the best station that is typically one of the nearest stations to the target site. In addition, the spatial distribution of the top four stations tends to become more spread as the return period level increases. This may be because for a longer return period level, earthquake magnitude becomes larger, and earthquake rupture area grows accordingly. In such cases, the station distribution that is more widely spread may be more effective in capturing the greater extent of the earthquake rupture area.

Finally, the performance of the sequential optimization approach is compared with that of the exhaustive combination approach by considering observation networks consisting of up to four stations. The results for the three return period levels are shown in Table 1. In the table, results for the exhaustive combination approach up to four stations are shown; in the bottom two lines (shaded with red color), the corresponding results for the sequential optimization approach are shown. The combinations identified by the sequential optimization approach are shaded with green color. For example, for the 200-year return period, the sequential optimization approach identifies the station ID [S_{98}, S_{52}, S_{27}, S_{46}] (in this order) as the quasi-optimal intensity-based index trigger system for Iwanuma. This is consistent with the results obtained from the exhaustive combination approach, where [S_{98}] as the best combination for the one-station case, [S_{98}, S_{52}] as the third-best combination for the two-station case, [S_{98}, S_{52}, S_{27}] as the second-best combination for the three-station case, and [S_{98}, S_{52}, S_{27}, S_{46}] as the best combination for the four-station case. For the 500-year return period, results based on the exhaustive combination approach and the sequential optimization approach coincide completely. The results shown in Table 1 indicate that for all three return period levels, the sequential optimization approach can identify the station combinations that are very close to the best combinations of the stations based on the exhaustive combination approach. Based on these results, the conclusions drawn in this section using the sequential optimization approach are considered as consistent and robust.

CONCLUSIONS

We developed new CAT-in-a-Box and intensity-based index trigger mechanisms for parametric tsunami catastrophe bonds to promote transfer of tsunami disaster risks to third parties via financial markets. The trigger conditions of the CAT-in-a-Box solutions are defined based on earthquake event characteristics (i.e., magnitude and location), whereas those for the intensity-based index solutions incorporate tsunami wave heights that are recorded at multiple observation stations. The calibration of the bond trigger mechanisms was based on the new probabilistic tsunami loss estimation method, which can capture the key uncertainties of tsunami hazard and risk processes by considering stochastic earthquake sources and state-of-the-art tsunami fragility and loss models. To ensure that the calibrated triggers are robust with regard to unseen data, ten-fold cross-validation was implemented in evaluating the performances of different trigger solutions. The proposed solutions were demonstrated for the realistic building portfolio in Iwanuma, Miyagi

Prefecture, Japan, by considering new and existing tsunami observation systems off the Tohoku coast, i.e., S-net and NOWPHAS, respectively, for the intensity-based index mechanisms.

From the numerical example of the case study, we draw the following conclusions:

1. CAT-in-a-Box solutions require higher magnitude thresholds for higher tsunami loss levels, and lead to more robust bond trigger performances (i.e., less local variability of the magnitude thresholds) when a larger sub-region size is considered. For the sub-region size of 50 km or more, 8% to 10% errors were achieved with relatively balanced situations for the average trigger errors using the fitting and testing data.
2. Single-station intensity-based index solutions identify stations that are relatively near the building portfolio or in offshore areas directly facing the target location as optimal observation points. When optimized, the single-station tsunami index can achieve the least average trigger errors of about 5% to 7%, depending on tsunami loss levels.
3. Multiple-station intensity-based index solutions indicate that inclusion of a few additional stations for defining the intensity-based index is particularly beneficial in reducing average trigger errors. When the observation network is optimized, average trigger errors of 3% to 4% can be achieved, which is significantly superior to those of the CAT-in-a-Box method.

The main conclusions from this study offer useful insight as to how more advanced intensity-based index solutions can be developed to other seismic regions with a smaller number of observation stations. However, caution should be exercised in applying the results of this study to other regions because the obtained results are strictly applicable to the considered case study region, and model risk (i.e., credibility of the tsunami risk model used for generating the data) has not been examined in this study. Calibration of the trigger mechanisms may be sensitive to various factors in the model (e.g., rupture source characteristics, regional topography, building portfolios, and tsunami fragility of buildings). Future studies should also address the development of parametric multi-hazard catastrophe bonds that are applicable to cascading earthquake-tsunami risks (Goda and De Risi 2018).

ACKNOWLEDGMENTS

The building stock data for Iwanuma were obtained from the tsunami damage database for the 2011 Tohoku Japan earthquake, maintained by the Ministry of Land Infrastructure and Transportation (http://www.mlit.go.jp/toshi/toshi-hukkou-arkaibu.html). This work is supported by the Leverhulme Trust (RPG-2017-006) for K. G. and J. S., Guy Carpenter for G. F., and the European Research Council (704679) for A. R.

APPENDIX

Please refer to the online version of this paper to access the supplementary material provided in the Appendix.

REFERENCES

Agresti, A., 2007. *An Introduction to Categorical Data Analysis*, John Wiley and Sons, Inc., Hoboken, NJ.

Cornell, C. A., and Krawinkler, H., 2000. Progress and challenges in seismic performance assessment, *PEER Center News* **3**, 1–4.

Cummins, D. J., 2008. CAT bonds and other risk-linked securities: State of the market and recent developments, *Risk Management and Insurance Review* **11**, 23–47.

De Risi, R., Goda, K., Yasuda, T., and Mori, N., 2017. Is flow velocity important in tsunami empirical fragility modeling? *Earth-Science Reviews* **166**, 64–82.

Franco, G., 2010. Minimization of trigger error in CAT-in-a-box parametric earthquake catastrophe bonds with an application to Costa Rica, *Earthquake Spectra* **26**, 983–998.

Fraser, S., Pomonis, A., Raby, A., Goda, K., Chian, S. C., Macabuag, J., Offord, M., Saito, K., and Sammonds, P., 2013. Tsunami damage to coastal defences and buildings in the March 11th 2011 Mw9.0 Great East Japan earthquake and tsunami, *Bulletin of Earthquake Engineering* **11**, 205–239.

Goda, K., 2013. Basis risk of earthquake catastrophe bond trigger using scenario-based versus station-intensity-based approaches: A case study for south-western British Columbia, *Earthquake Spectra* **29**, 757–775.

Goda, K., 2015. Seismic risk management of insurance portfolio using catastrophe bonds, *Computer-Aided Civil and Infrastructure Engineering* **30**, 570–582.

Goda, K., and Atkinson, G. M., 2014. Variation of site-to-source distance for mega-thrust subduction earthquakes: Effects on ground motion prediction equations, *Earthquake Spectra* **30**, 845–866.

Goda, K., and De Risi, R., 2017. Probabilistic tsunami loss estimation: Stochastic earthquake scenario approach, *Earthquake Spectra* **33**, 1301–1323.

Goda, K., and De Risi, R., 2018. Multi-hazard loss estimation for shaking and tsunami using stochastic rupture sources, *International Journal of Disaster Risk Reduction* **28**, 539–554.

Goda, K., Mai, P. M., Yasuda, T., and Mori, N., 2014. Sensitivity of tsunami wave profiles and inundation simulations to earthquake slip and fault geometry for the 2011 Tohoku earthquake, *Earth Planet Space* **66**, 105.

Goda, K., Yasuda, T., Mori, N., and Maruyama, T., 2016. New scaling relationships of earthquake source parameters for stochastic tsunami simulation, *Coastal Engineering Journal* **58**, 1650010.

Goto, C., Ogawa, Y., Shuto, N., and Imamura, F., 1997. *Numerical method of tsunami simulation with the leap-frog scheme, IOC Manual, No*. 35, United Nations Educational, Scientific and Cultural Organization (UNESCO), Paris, France.

Goulet, C. A., Haselton, C. B., Mitrani-Reiser, J., Beck, J. L., Deierlein, G. G., Porter, K. A., and Stewart, J. P., 2007. Evaluation of the seismic performance of a code-conforming reinforced-concrete frame building - From seismic hazard to collapse safety and economic losses, *Earthquake Engineering & Structural Dynamics* **36**, 1973–1997.

Headquarters for Earthquake Research Promotion, 2013. Investigations of future seismic hazard assessment, Tokyo, Japan, 217 p.

Kanazawa, T., 2013. Japan Trench earthquake and tsunami monitoring network of cable-linked 150 ocean bottom observatories and its impact to earth disaster science, *2013 IEEE Intl. Underwater Technology Symposium*, doi:10.1109/UT.2013.6519911.

Kawai, H., Satoh, M., Kawaguchi, K., and Seki, K., 2013. Characteristics of the 2011 Tohoku tsunami waveform acquired around Japan by NOWPHAS equipment, *Coastal Engineering Journal* **55**, 1350008.

Kim, J. H., 2009. Estimating classification error rate: Repeated cross-validation, repeated hold-out and bootstrap, *Computational Statistics & Data Analysis* **53**, 3735–3745.

King, A., Middleton, D., Brown, C., Johnston, D., and Johal, S., 2014. Insurance: Its role in recovery from the 2010-2011 Canterbury earthquake sequence, *Earthquake Spectra* **30**, 475–491.

Løvholt, F., Glimsdal, S., Harbitz, C. B., Horspool, N., Smebye, H., de Bono, A., and Nadima, F., 2014. Global tsunami hazard and exposure due to large co-seismic slip, *International Journal of Disaster Risk Reduction* **10**, 406–418.

Mitchell-Wallace, K., Jones, M., Hillier, J., and Foote, M., 2017. *Natural Catastrophe Risk Management and Modelling: A Practitioner's Guide*, Wiley-Blackwell, Hoboken, NJ, 536 p.

Mossin, J., 1968. Aspects of rational insurance purchasing, *Journal of Political Economy* **91**, 304–311.

Okada, Y., 1985. Surface deformation due to shear and tensile faults in a half-space, *Bulletin of the Seismological Society of America* **75**, 1135–1154.

Pardo-Iguzquiza, E., and Chica-Olmo, M., 1993. The Fourier integral method: An efficient spectral method for simulation of random fields, *Mathematical Geology* **25**, 177–217.

Pucciano, S., Franco, G., and Bazzurro, P., 2017. Loss predictive power of strong motion networks for usage in parametric risk transfer: Istanbul as a case study, *Earthquake Spectra* **33**, 1513–1531.

Satake, K., Fujii, Y., Harada, T., and Namegaya, Y., 2013. Time and space distribution of coseismic slip of the 2011 Tohoku earthquake as inferred from tsunami waveform data, *Bulletin of the Seismological Society of America* **103**, 1473–1492.

Schlesinger, H., 2000. The theory of insurance demand, in *Handbook of Insurance* (G. Dionne, ed.), Kluwer Academic Publishers, Boston, MA, 131–151.

Tanioka, Y., and Satake, K., 1996. Tsunami generation by horizontal displacement of ocean bottom, *Geophysical Research Letters* **23**, 861–864.

Wald, D. J., and Franco, G., 2016. Money matters: Rapid post-earthquake financial decision-making, *Natural Hazards Observer* **XL**(**7**), 24–27.

(Received 9 March 2018; Accepted 15 June 2018)